

Bimodal Distribution of Magnetic Fields and Areas of Sunspots

Andrey G. Tlatov¹ · Alexei A. Pevtsov²

Received: 9 Jan 2013 / Accepted: 31 July 2013 / Published online: ●●●●●●●●●●

Abstract We applied automatic identification of sunspot umbrae and penumbrae to daily observations from the *Helioseismic Magnetic Imager* (HMI) on board the *Solar Dynamics Observatory* (SDO) to study their magnetic flux (B) and area (A). The results confirm a previously known logarithmic relationship between the area of sunspots and their maximum flux density. In addition, we find that the relation between average magnetic flux (B_{avg}) and sunspot area shows a bimodal distribution: for small sunspots and pores ($A \leq 20$ millionth of solar hemisphere, MSH), $B_{\text{avg}} \approx 800$ G (gauss), and for large sunspots ($A \geq 100$ MSH), B_{avg} is about 600 G. For intermediate sunspots, average flux density linearly decreases from about 800 G to 600 G. A similar bimodal distribution was found in several other integral parameters of sunspots. We show that this bimodality can be related to different stages of sunspot penumbra formation and can be explained by the difference in average inclination of magnetic fields at the periphery of small and large sunspots.

Keywords: Sun: surface magnetism, Sunspots, Sun: activity

1. Introduction

Sunspots are the longest studied activity phenomena on the Sun. Recent advances in high resolution observations and numerical modeling have brought a better understanding of fine structure of individual sunspots, their emergence, and evolution. Still, knowledge of statistical properties of sunspots is important for understanding of their physical characteristics as a distinct “family” of solar features, which in turn could be invaluable for modeling of this solar phenomenon. Some of the oldest records of sunspot statistical properties include their coordinates and area (*e.g.*, Hathaway, 2010), with a later addition of sunspot contrast and magnetic field strengths (*e.g.*, Solanki, 2003). All these previous data are based on ground-based observations, which are subject to

¹ Kislovodsk Solar Station of Pulkovo Observatory, PO Box 145, Gagarina Str., 100, Kislovodsk, 357700 Russian Federation email: tlatov@mail.ru

² National Solar Observatory, Sunspot, NM 88349, U.S.A. email: apevtsov@nso.edu

atmospheric image distortion, interruption due to day-night cycle, and weather conditions. The launch of *Solar Dynamics Observatory* (SDO) with the *Heliioseismic Magnetic Imager* (HMI; Scherrer *et al.*, 2012) on board brings the studies of statistical properties of sunspots to a new level by providing nearly simultaneous observations of magnetic fields and Doppler velocities with high spatial resolution and cadence. High (uniform) quality imaging observations from space also enable automatic identification of solar features. This work employs the HMI observations taken during 2010-2012 to study statistical properties of sunspots such as their area and magnetic field. To identify sunspots, we use an automatic method developed by Tlatov *et al.* (2013). The data and their analysis are briefly described in Section 2. The magnetic field and area of sunspots (presented in Section 3) show a clear presence of two “sub-families” of sunspots with distinct average properties. In Section 4 we discuss these findings.

2. Data and Analysis Method

To identify sunspots, we employ the method developed by Tlatov *et al.* (2013). Previously, the method was applied to ground-based data from Kislovodsk Solar Station and space-borne observations from SOHO/MDI. It showed a very good agreement with manual and semi-automatic sunspot identifications. More recently, the method was compared with STARA sunspot catalogue (Watson *et al.*, 2009), and the agreement was found to be excellent (A. Tlatov, 2012, private communication). The method was further modified to allow the identification of multiple umbrae inside a common penumbra.

To determine the outer (quiet sun–penumbra) and inner (penumbra–umbra) penumbral boundaries we employ two known methods: intensity threshold (*e.g.*, Watson *et al.*, 2009) and the border (gradient) method (*e.g.*, Zharkova *et al.*, 2005). First, a potential sunspot is identified using an intensity threshold relative to a limb-darkening function fitted to the data. For pixels below the threshold, we apply a growing procedure; we add pixels to form a closed boundary around the sunspot candidate if the intensity contrast for these pixels falls within the range of specified contrast. The contrast range for this step was determined by a trial-and-error approach. After the outer boundary of the sunspot is defined, we use the distributions of intensity and contrast in pixels inside of that closed boundary to identify the penumbra–umbra boundary. Light bridges are included in the total area of the sunspot, but they are excluded from umbral areas. For additional details of this method, we refer the reader to Tlatov *et al.* (2013). For the analysis presented in this article, we correct sunspot areas for foreshortening.

We use daily observations from SDO/HMI taken in quasi-continuum (filenames hmi.Ic.45s) during June 2010 – September 2012. To minimize the size of data set and mitigate the effect of spacecraft’s orbital motions, only one image per day (taken at 5:00 UT) is used. The total number of features identified during the above period is 14094 sunspots and pores. To minimize the projection effects, we further limit the data set to features found within 30° from solar disk center ($\mu = \sin \rho \leq 0.5$, where ρ is angular heliocentric distance). Next, we classified all features into pores and sunspots. Features for which the area of the umbra

is equal to its total area are classified as pores and features with penumbra are classified as sunspots, respectively. Thus, the final data set consists of 4648 features: 3027 pores and 1621 sunspots.

An error analysis of HMI longitudinal magnetograms was published by Liu *et al.* (2012). From this analysis, an upper limit for random noise in HMI longitudinal magnetograms is about 10 Mx (maxwell) $\text{cm}^{-2} = 10 \text{ G}$ (gauss) for 45-second magnetograms (same type of magnetograms as used by us). The noise increases slightly as a function of heliocentric distance. In addition, strong fields measured in sunspots exhibit a 24-h modulation, which means that for higher orbital velocities (relative to the Sun) the calibration curve for longitudinal magnetograms becomes less accurate. To mitigate the effect of orbital motions, we only select one magnetogram per day taken at about 5:00 UT. However, this approach does not completely eliminate the effects of spacecraft orbital motions. On average, the amplitude of magnetic flux variations due to orbital motions is about 2.7% of the measured flux (Liu *et al.*, 2012). An example in Liu *et al.* (2012) (see their Figure 5) shows residual variations in the amplitude of field ranging from about 50 to 140 G (for the observed longitudinal fields in the range of 1000–1200 G). These daily variations in strong flux contribute to scatter in B_{MAX} shown in our Figure 1. In fact, after subtracting a fitted functional dependence from data points shown in Figure 1, the residual scatter is about 120–140 G, which is in qualitative agreement with Liu *et al.* (2012). Such daily variations in magnetic flux will only affect B_{MAX} , but not sunspot areas.

After identifying sunspots and pores, their boundaries were superposed onto the longitudinal magnetograms taken by HMI simultaneously with the quasi-continuum images. Magnetograms were used to compute the total magnetic flux Φ and the maximum magnetic flux density (B_{MAX}). In these calculations, we corrected the observed magnetic field by $\cos \rho$. Limiting the data set to $\rho \leq 30^\circ$ also helps in minimizing the effects of projection. Magnetic flux density is a product of field strength, cosine of inclination angle (relative to the line-of-sight) and the fill factor (fraction of a pixel occupied by magnetized plasma). As the magnetic field is close to vertical in sunspot umbrae, and the fill factor is close to unity there, the observed longitudinal flux density corrected for $\cos \rho$ may serve as a good proxy for true field strength except for areas of very strong magnetic fields where longitudinal magnetograms may exhibit magnetic saturation (Hagyard and Pevtsov, 1999). According to Liu *et al.* (2012) SDO/HMI longitudinal magnetograms may saturate when the field strength exceeds 3200 G. During the 2010-2012 period included in our study, very few sunspots were measured having their field strength in excess of 3200 G (based on measurements of field strength by W. Livingston in Fe I 1565 nm). Pietarila *et al.* (2013) found good correlation between longitudinal magnetograms from Vector Spectro-Magnetograph (VSM) on the *Solar Optical Investigation of the Sun* (SOLIS) suite of instruments and SDO/HMI, although their correlation varies across solar disk.

To further demonstrate that the longitudinal field provides a reasonable proxy for true field strength in sunspot umbra, we use observations of active region NOAA 7926 (18–25 November 1995) taken with the Advanced Stokes Polarimeter equipped on the Dunn Solar Telescope of the National Solar Observatory,

Sacramento Peak. Magnetic fields were derived via inversion of Stokes profiles in the framework of Milne-Eddington model of stellar atmospheres following Skumanich and Lites (1987). In two magnetograms taken three days apart, the maximum field strengths derived by correcting the line-of-light flux by the cosine of the heliocentric distance ρ were 1872 G and 1586 G. The corresponding field strengths derived from full Stokes profile inversion (taking into account the fill factor) were 1969 G and 1311 G, or within 5–20% of the field strength proxy derived from the longitudinal magnetograms.

The correction using cosine of heliocentric angle works reasonably well for umbral magnetic fields which are more vertical. In the sunspot penumbra, the magnetic fields become more horizontal. Thus, the total and average fluxes that we discuss in later sections refer to the vertical flux.

3. Relation between Magnetic Flux and Sunspot Area

Several studies (*e.g.*, Houtgast and van Sluiter, 1948; Rezaei, Beck, and Schmidt, 2012) found a correlation between the area of sunspots (A , in millionth of solar hemisphere, MSH) and their recorded maximum field strength. Ringnes and Jensen (1960) found the strongest correlation between the logarithm of area and the field strength.

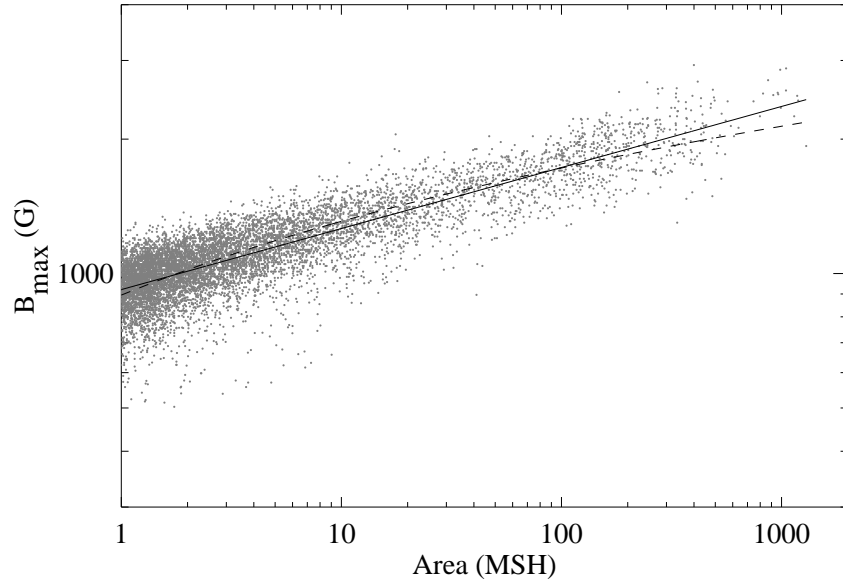


Figure 1. Maximum field strength (B_{MAX}) *vs.* area (A) of pores and sunspots. The black solid line shows the least-squares fit $\log B_{\text{MAX}} = (2.9640 \pm 0.0008) + (0.1367 \pm 0.0009) \times \log A$ to the data. The dashed line corresponds to a fit $B_{\text{MAX}} = (894.7640 \pm 2.1067) + (414.1450 \pm 2.458) \times \log A$.

Figure 1 shows a scatter plot between maximum field strength (B_{MAX}) in sunspot/pore and sunspot area (A). Two least-squares fits were made to the data: $\log B_{\text{MAX}} = (2.9640 \pm 0.0008) + (0.1367 \pm 0.0009) \times \log A$ (the solid line in Figure 1) and $B_{\text{MAX}} = (894.7640 \pm 2.1067) + (414.1450 \pm 2.458) \times \log A$ (the dashed line). The F -test indicates that both of these models fit the data equally well. Pearson’s correlation coefficient $r_P=0.8731$ is slightly higher for $\log A$ – linear B_{MAX} as compared with the $r_P=0.8410$ for $\log A$ – $\log B_{\text{MAX}}$ relationship. However, visually, it appears that $\log A$ – linear B_{MAX} fit works well only for the range of smaller areas and lower field strengths. The $\log A$ – $\log B_{\text{MAX}}$ fit works well for all ranges in area and field strength. Pevtsov *et al.* (2013) noted possible correlation between the steepness of the $\log A$ – $\log B_{\text{MAX}}$ relation and the amplitude of the next solar cycle. The solar-cycle dependence of the $\log A$ – linear B_{MAX} relationship was described by Ringnes and Jensen (1960), who found the following scaling coefficients; for 1917–1924 (cycle 15): 980, 1924–1934 (cycle 16): 970, 1934–1944 (cycle 17):1410, 1945–1954 (cycle 18):1610, and 1954–1956 (rise of cycle 19):1710. The amplitudes of sunspot cycles progressively increase from cycle 15 to cycle 19. If the scaling coefficient derived from the fitted relationship in Figure 1 follows the above trend, solar cycle 24 is expected to be much lower in amplitude than cycles 15 and 16, which is in agreement with the current predictions for cycle 24.

While there is no physical model explaining the observed relationship between the magnetic field and area of sunspots, $\log A$ – $\log B_{\text{MAX}}$ relationship can be derived from the distribution of the magnetic field of a dipole situated at a certain depth below the photosphere (Ikhsanov, 1968). The dipole field was found to be a good representation of sunspot magnetic field (Bumba, 1960; Skumanich, 1992).

Figure 2 shows a scatter plot between total magnetic flux (Φ) and sunspot/pore area (A). As the location of pores and small sunspots partially overlaps in this plot, their approximate ranges in size are identified by horizontal bars. The smallest sunspots in our data set have an area of about 4.5 MSH, which corresponds to a circular feature of about 4.2 Mm in diameter. The largest pores have an area of about 19 MSH, which corresponds to a circular feature of approximately 8.5 Mm in diameter. For comparison, the smallest sunspots reported by Bray and Loughhead (1964) were about 3.5 Mm in diameter, and the largest pores were observed to be of 7 Mm in diameter. In the following discussion, we refer to sunspots with $A < 20$ MSH as small sunspots and to those with $A > 100$ MSH as regular sunspots. The area between 20 and 100 MSH is referred to as the transition sunspots. The data shown in Figure 2 include 3027 pores, 624 small sunspots, 560 transition sunspots, and 437 regular sunspots. The selection of ranges for separating small, transition, and regular sunspots is based on the transitions between these sunspots clearly identifiable in Figure 2.

Figure 2 shows one peculiar feature that, perhaps, deserves a separate explanation. The scatter in flux (in the y -direction) is asymmetric: it only extends towards the lower values, while there appears to be an upper limit in it. We attribute this to a residual effect of the spacecraft orbital motions. As Liu *et al.* (2012) showed, the magnetic flux measured in a sunspot varies with 24-h periodicity. In this variation, the measurements taken on the same sunspot during a single day will be equal to or systematically lower than the “true” flux of that

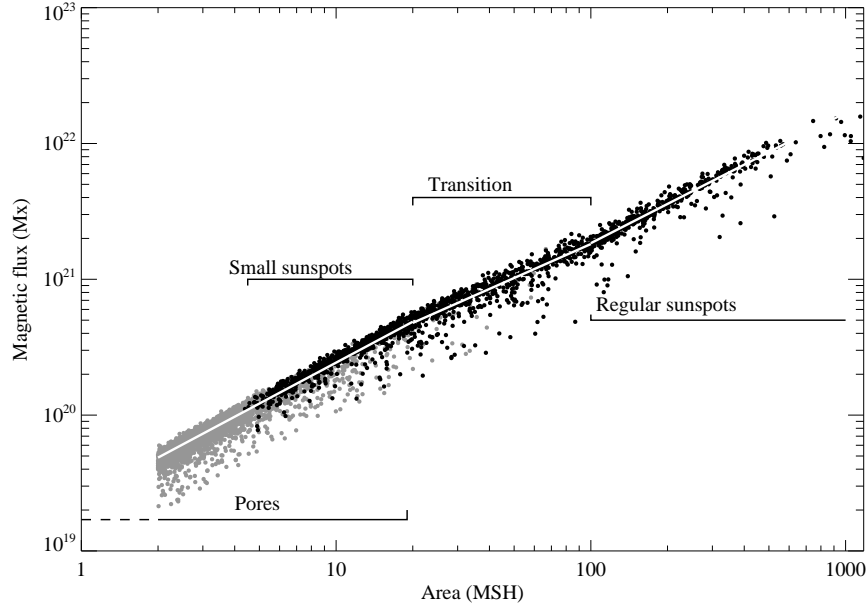


Figure 2. Total magnetic flux as a function of the area of pores (gray) and sunspots (black). Because pores and small sunspots partially overlap, horizontal bars mark approximate range in their areas. Also marked are ranges for regular sunspots and transition between small and regular sunspots. Three straight (white) lines plotted over the data points correspond to linear fits to the data for areas smaller than 20 MSH (pores and small sunspots), between 20 and 100 MSH (transition), and larger than 100 MSH (regular sunspots).

sunspot. At the same time, sunspot areas will not be affected by orbital motions. Thus, the upper limit in magnetic flux in Figure 2 represents the “true” value of magnetic flux for measured features, and asymmetric scatter extending below that “true” value is due to systematic variations associated with orbital motions. A similar upper limit can also be seen in Figure 1, although it is much less clear in comparison with Figure 2.

Although Figure 2 looks very similar to Figure 1, there is one important difference: the slope is different for areas smaller than about 20 MSH and for those larger than 100 MSH. A linear fit to the area–flux relationship in Figure 2 shows a clear change between small and transition sunspots, and between transition and regular sunspots (compare inclination of three linear segments fitted to the data in Figure 2). If one has to fit a continuous function to the data in Figure 2, it appears that an $A \sin(\log A)$ function fits reasonably well. The curve corresponding to this function will overlap with three linear segments shown in Figure 2, and thus, is not shown in Figure 2.

The ranges for “small” and “regular” sunspots are not exact and thus, they do have some small degree of uncertainty. This uncertainty, however, has no effect on our conclusions.

The transition from one slope to the other is more profound in the relationship between area A and average magnetic flux B_{avg} (Figure 3). For pores, B_{avg}

slightly increases with area, albeit with significant scatter in the data. For small sunspots, the average magnetic flux stays constant at approximately 850 G, and for regular sunspots $B_{\text{avg}} \approx 600$ G. For transition sunspots, B_{avg} decreases with sunspot area almost linearly.

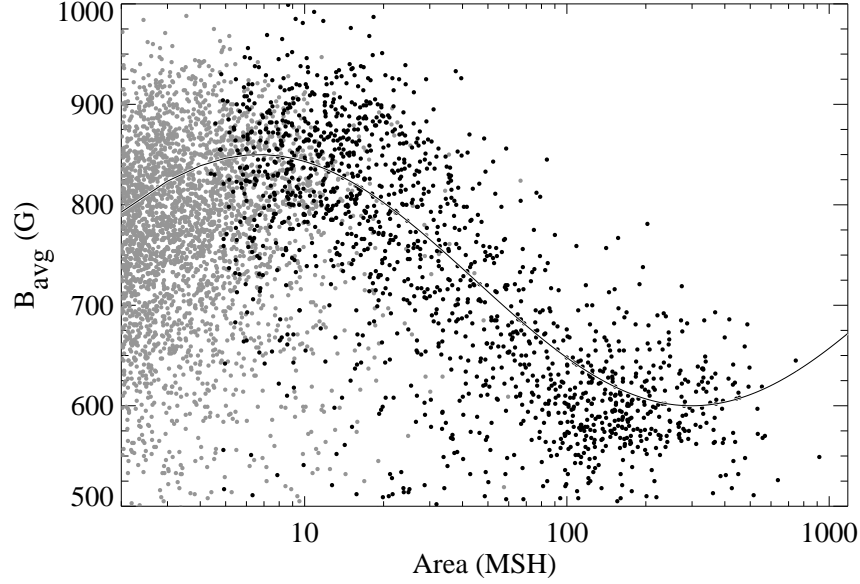


Figure 3. Average magnetic flux *vs.* area of pores (gray dots) and sunspots (black dots). The thin solid line corresponds to a $\sin(\log A)$ function.

4. Bimodal Distribution of Sunspots

Geometric properties of “small” and “regular” sunspots form two distinct groups. Figure 4a shows the distributions of the ratio A_u/A_s between the area of sunspot umbra (A_u) and the total area of sunspot (A_s) for three groups. For regular sunspots, the distribution is very narrow, and it peaks at about $A_u/A_s = 0.156 \pm 0.034$. This is in agreement with previous studies, *e.g.*, $A_u/A_s = 0.168$ – 0.175 in Antalova (1991) and references therein (the above values were derived from the ratio of the radii of umbra and sunspot listed in Table 1 of Antalova, 1991). Some of these previous studies suggest that the umbra/sunspot area ratio changes with sunspot field strength (Antalova, 1991). On the other hand, no variation in A_u/A_s with solar cycle was found by Beck and Chapman (1993).

For small sunspots, the distribution of A_u/A_s ratio is very broad with the average of 0.359 ± 0.119 . For transition sunspots, $A_u/A_s = 0.231 \pm 0.099$ (see Figure 4a). This can also be seen in Figure 4b, which shows the relationship between the area of umbra and area of sunspot.

A narrow width of the distribution of A_u/A_s for regular sunspots suggests lack of dependence of the area ratio on the field strength for these sunspots.

The bimodal distribution is present in several other parameters. For example, the relationship between B_{MAX} in sunspots and average magnetic flux density in penumbra ($B_{\text{avg,p}}$) shows two distinct tendencies: for smaller sunspots with $A_s \leq 50$ MSH, $B_{\text{avg,p}}$ increases with B_{MAX} . For larger sunspots with $A_s > 50$ MSH, $B_{\text{avg,p}}$ stays nearly constant at about 500 G, independent of B_{MAX} . The ratio of areas A_u/A_s vs. the ratio of fluxes in the umbra (Φ_u) and in the entire sunspot (Φ_s) also forms two distinct relationships for smaller and larger sunspots. Due to space limitations, these other relationships are not shown as graphs.

5. Discussion

Our analysis of properties of sunspots automatically selected in SDO/HMI daily images confirms the logarithmic relationship between maximum magnetic field strength in sunspots and their total area. Both $\log - \log$ and $\log - \text{linear}$ functional relationships fit the data relatively well, although $\log - \log$ least-squares fit appears to work better. Although several studies had established a strong correlation between the area of sunspots and their maximum field strength, the nature of this relationship is not well understood. In addition, the measurements of (maximum) magnetic fields may differ between instruments, while the measurements of areas are more instrument independent. For example, scattered light and strong blending in the Ni I 676.8 nm line in the umbrae of sunspots could be a factor for B_{MAX} measurements for some instruments (*e.g.*, MDI). These factors could result in a different $\log A - \log B_{\text{MAX}}$ relationship as found by us.

We also find a bimodal distribution of properties of sunspots, depending on their size. Small sunspots and pores follow the same relationship between the magnetic flux and area. We see a significant overlap in size and flux between these two solar features. This suggests that small sunspots may originate from pores, and not develop as independent features. The scenario that sunspots evolve from pores was previously proposed by several researchers (Rucklidge, Schmidt, and Weiss, 1995; Skumanich, 1999). In particular, Rucklidge, Schmidt, and Weiss (1995) suggested that when a pore reaches a critical size, it will abruptly make a transition to a sunspot. Indeed, our data indicate a transition between small (rudimentary) sunspots and regular sunspots. However, the shape of transition is rather gradual, which is different from a hysteresis-type transition as in Rucklidge, Schmidt, and Weiss (1995) model. Interestingly, functional relationship between sunspot radius and magnetic flux based on the $\sin(\log A)$ function fitted to Figure 3 is similar to the one shown in Figure 4 of Skumanich (1999). By itself, the choice of $\sin(\log A)$ function was made arbitrary based on a visual fit to the data in Figure 3. While we have no physics-based explanation for this functional form, we note that it represents the $\log A - \log \Phi$ relationship in Figure 2 quite well. Although not shown in Figure 2, the umbrae of sunspots follow the same trend as small sunspots and pores. For umbrae, the trend continues through the area occupied by “transition” sunspots, but unlike sunspots, the umbrae do not change the slope of $\log A - \log \Phi$ relationship.

The transition between small and regular sunspots may be associated with the formation of regular penumbra. When the sunspot penumbra starts forming, the magnetic field becomes more horizontal, and thus, the relation between the vertical flux and the area of sunspot changes. This change corresponds to transition sunspots in Figure 2. For sunspots with fully developed penumbra, the ratio between the areas of umbra and sunspot as a whole remains constant even though the sunspots may continue to grow in size. These changes in flux–area and umbra–sunspot area correlations are in a qualitative agreement with the scenarios of sunspot formation described, *e.g.*, by Zwaan (1992) and Rezaei, Beck, and Schmidt (2012). Collados *et al.* (1994) studied three sunspots with well-developed penumbra, and found systematic differences in sunspots of different size. They concluded that sunspots with small and large umbrae may require different models to represent their atmospheres.

The longitudinal field is a projection of full vector field to the line-of-sight direction. Thus, it is possible to derive some information about the inclination of vector field to solar surface from the line-of-sight data, albeit with some restrictive assumptions. For example, one can assume that the magnetic field in a sunspot does not change significantly over several days as it travels across the solar disk. In the framework of that simple model, the line-of-sight field will show a different evolution depending on the inclination of vector field to solar surface. Below we exploit this approach to demonstrate that the inclination of magnetic field at the periphery of sunspots is different for sunspots of different size.

Figure 5 shows the ratio of the magnetic field in the disk center side of the penumbra at the distance of $2/3$ of sunspot radius from the center of sunspot ($B_{2/3}$) to the magnetic field at the center of sunspot (B_c) as a function of heliocentric distance $\mu = r/R$. (Here we compare only magnetic fields in the disk center side of penumbra and at sunspot center to avoid potential issues with polarity reversal of magnetic field at the periphery of sunspots due to projection effects). For this plot, we include all identified sunspots up to $\mu = 0.98$. As a reminder, the data discussed earlier were limited to $\mu \leq 0.5$. Next, we computed median values of $B_{2/3}/B_c$ within ± 0.1 intervals centered at $\mu = 0.1, 0.3, 0.5, 0.7$, and 0.9 . For small sunspots (triangles in Figure 5), $A_s \leq 20$ MSH), the ratio $B_{2/3}/B_c$ is about 0.9, and it does not vary significantly with the heliocentric distance. This indicates that on average, the magnetic fields are nearly vertical in smallest sunspots. Transition sunspots with areas $20 \text{ MSH} < A < 100 \text{ MSH}$ show a small variation in $B_{2/3}/B_c$ with μ . And for regular sunspots, this variation with the heliocentric distance is much stronger. Since we use the line-of-sight (LOS) magnetograms, B_c will vary with heliocentric angle as $B_c^{\text{LOS}} = B_c \cos \rho$, where ρ is angular heliocentric distance (this assumes that the magnetic field is vertical at the center of the sunspot). For a magnetic field inclined from the vertical direction by an angle γ , the LOS component can be expressed as $B^{\text{LOS}} = B \cos(\gamma - \rho)$. Therefore,

$$\frac{B_{2/3}^{\text{LOS}}}{B_c^{\text{LOS}}} = \frac{B_{2/3} \cdot \cos(\gamma - \rho)}{B_c \cdot \cos \rho} = \frac{B_{2/3}}{B_c} (\cos \gamma + \sin \gamma \cdot \tan \rho).$$

The least-squares fit to the data by this function returns progressively larger inclination angles in sunspot penumbra (at the distance of $\frac{2}{3}R_s$ from sunspot center): $\approx 1^\circ$ (small sunspots), 15° (transition sunspots), and 38° (regular sunspots).

The difference in average inclination of penumbral magnetic field (at $\frac{2}{3}R_s$) between small, intermediate, and regular sunspots supports our early suggestion that the bimodal distribution of properties of sunspots may be associated with different stages of sunspot formation. Small sunspots may have rudimentary and irregular penumbra, which has not yet evolved to a regular penumbra with more horizontal fields as in regular sunspots. In transition sunspots (A between 20 and 100 MSH), the average inclination of magnetic fields in the penumbra increases, and rapidly, fields become more horizontal.

The change in the inclination of vector field for sunspots at different stages of its development was observed using data from the Advanced Stokes Polarimeter (using magnetograms of active region NOAA 7926 described in Section 2). The main sunspot in this active region was decaying over the period of observations. On the day when the sunspot had a well-developed penumbra, the average inclination of vector magnetic field in the penumbra (at about $2/3$ of the sunspot radius) was about $25\text{--}30^\circ$, while in the umbra the field was nearly vertical (the inclination angle of about 80°). Three days later, when this sunspot lost most of its penumbra, the inclination of magnetic field in the umbra did not change, but the field at $2/3$ of radius of the sunspot became more vertical (the inclination increased to $55\text{--}60^\circ$). While this is a single example, it supports our inferences about difference in inclination of magnetic field in sunspots with different stages of penumbral development.

Vitinsky, Kopecký and Kuklin (1986) (see also, Dmitrieva, Kopecký, and Kuklin, 1968) reported that the distribution of areas of sunspots shows two distinct peaks. One maximum in that distribution corresponded to areas of about 8–13 MSH. Vitinsky, Kopecký and Kuklin (1986) associated this maximum with the location of small sunspots often developing in inter supergranular spaces (vertices), where the boundaries of three supergranules meet together. The second maximum in the size distribution was found at $A = 100\text{--}150$ MSH, which corresponds to an approximate size of supergranules. Recently, Nagovitsyn, Pevtsov, Livingston (2012) reported similar bimodal distribution of sunspot areas. Following the arguments given by Vitinsky, Kopecký and Kuklin (1986), for small sunspots located at the vertices of supergranular cells, there is an additional force from converging supergranular flows (as well as a strong downflow at the vertex location), which may result in increased average magnetic field in small sunspots and pores. When sunspots grow and get comparable in size with a supergranule, this additional force decreases. These early ideas need to be further verified with more recent modeling and observations. Finally, the results presented in this article are derived using longitudinal magnetograms. Additional studies based on high spatial resolution vector magnetograms may further improve the understanding of the bimodal distribution of sunspots reported here.

Acknowledgements A.G.T. acknowledges support by the Russian Foundation for Basic Research (RFBR) and the Russian Academy of Sciences (RAS). The National Solar Observatory is operated by the Association of Universities for Research in Astronomy (AURA), Inc. under a cooperative agreement with the National Science Foundation.

References

- Antalova, A.: 1991, *Bull. Astron. Inst. Czechosl.* **42**, 316.
- Beck, J.G., Chapman, G.A.: 1993, *Solar Phys.* **146**, 49.
- Bray, R. J., Loughhead, R. E.: 1964, *Sunspots*, Chapman and Hall, London, 70.
- Bumba, V.: 1960, *Izv. Krym. Astrofiz. Obs.* **23**, 134.
- Collados, M., Martinez Pillet, V., Ruiz Cobo, B., del Toro Iniesta, J.C., Vazquez, M.: 1994, *Astron. Astrophys.* **291**, 622.
- Dmitrieva, M.G., Kopecký, M., Kuklin, G.V.: 1968, In: Kiepenheuer, K.O. (ed.) *Structure and Development of Solar Active Regions*, IAU Symp **35**, 174.
- Ikhsanov, R.N.: 1968, *Soviet Astron.* **11**, 843.
- Hagyard, M.J., Pevtsov, A.A.: 1999, *Solar Phys.* **189**, 25.
- Hathaway, D.H.: 2010, *Living Rev. Solar Phys.* **7**, (1), <http://solarphysics.livingreviews.org/Articles/lrsp-2010-1/>.
- Houtgast, J., van Sluiter, A.: 1948, *Bull. Astron. Inst. Netherlands* **10**, 325.
- Liu, Y., Hoeksema, J.T., Scherrer, P.H., Schou, J., Couvidat, S., Bush, R.I., Duvall, T.L., Hayashi, K., Sun, X., Zhao, X.: 2012, *Solar Phys.* **279**, 295.
- Nagovitsyn, Yu. A., Pevtsov, A.A., Livingston, W.C.: 2012, *Astrophys. J. Lett.* **758**, L20.
- Pevtsov, A. A., Bertello, L., Tlatov, A., Kilcik, A., Nagovitsyn, Y., Cliver, E. W.: 2013, *Solar Phys.*, doi: 10.1007/s11207-012-0220-5.
- Pietarila, A., Bertello, L., Harvey, J.W., Pevtsov, A.A.: 2013, *Solar Phys.* **282**, 91.
- Rezaei, R., Beck, C., Schmidt, W.: 2012, *Astron. Astrophys.* **541**, A60.
- Ringnes, T. S., Jensen, E.: 1960, *Astrophys. Norvegica* **7**, 99.
- Rucklidge A. M., Schmidt, H. U., Weiss, N. O.: 1995, *Mon. Not. Roy. Astron. Soc.* **273**, 491.
- Scherrer, P.H., Schou, J., Bush, R.I., Kosovichev, A.G., Bogart, R.S., Hoeksema, J.T., et al.: 2012, *Solar Phys.* **275**, 207.
- Skumanich, A.: 1992, In: Thomas, J.H., Weiss, N.O. (eds.), *Sunspots: Theory and Observations*, NATO ASI Series C **375**, Kluwer Academic Publishers, Dordrecht, 121.
- Skumanich, A.: 1999, *Astrophys. J.* **512**, 975.
- Skumanich, A., Lites, B.W.: 1987, *Astrophys. J.* **322**, 473.
- Solanki, S.K.: 2003, *Astron. Astrophys. Rev.* **11**, 153.
- Tlatov, A. G., Vasil'eva, V. V., Makarova, V. V., Otkidychev, P., A.: 2013, *Solar Phys.* in press.
- Vitinsky, Yu. I., Kopecký, M., Kuklin, G. V.: 1986, *The Statistics of Sunspots (Statistika Pjatoobrazovatelnoj Dejatelnosti Solntsa)*, Nauka, Moscow, 397 (in Russian).
- Watson, F., Fletcher, L., Dalla, S., Marshall, S.: 2009, *Solar Phys.* **260**, 5.
- Zharkova, V.V., Aboudarham, J., Zharkov, S., Ipson, S.S., Benkhalil, A.K., Fuller, N.: 2005, *Solar Phys.* **228**, 361.
- Zwaan, C.: 1992, In: Thomas, J.H., Weiss, N.O. (eds.), *Sunspots: Theory and Observations*, NATO ASI Series C **375**, Kluwer Academic Publishers, Dordrecht, 75.

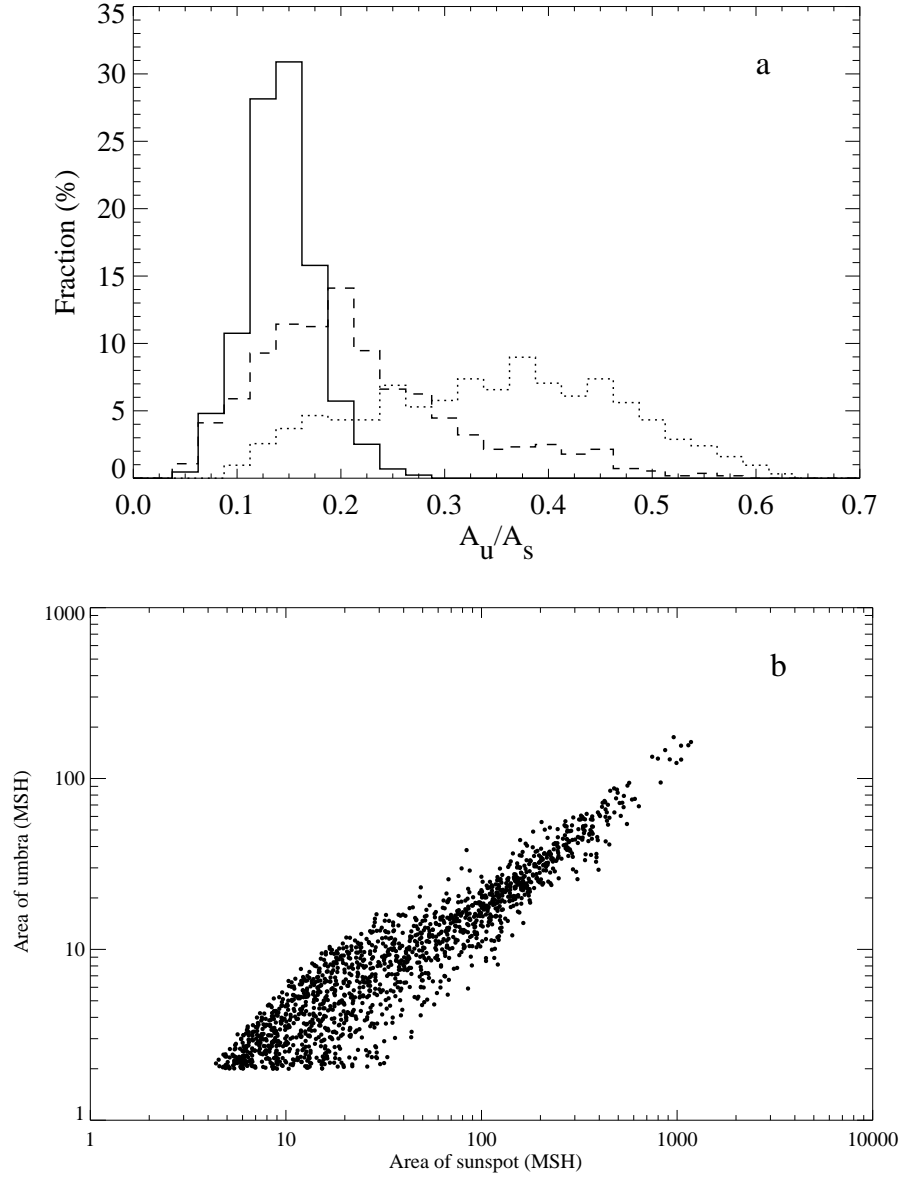


Figure 4. (a) Normalized distributions of the ratio of umbral area (A_u) to total sunspot area (A_s) for regular sunspots (solid line, $A_s \geq 100$ MSH), transition sunspots (dashed, $20 \text{ MSH} < A_s < 100 \text{ MSH}$) and rudimentary (small) sunspots (dotted, $A_s \leq 20 \text{ MSH}$). (b) The area of umbra (A_u) vs. the total area of sunspot (A_s).

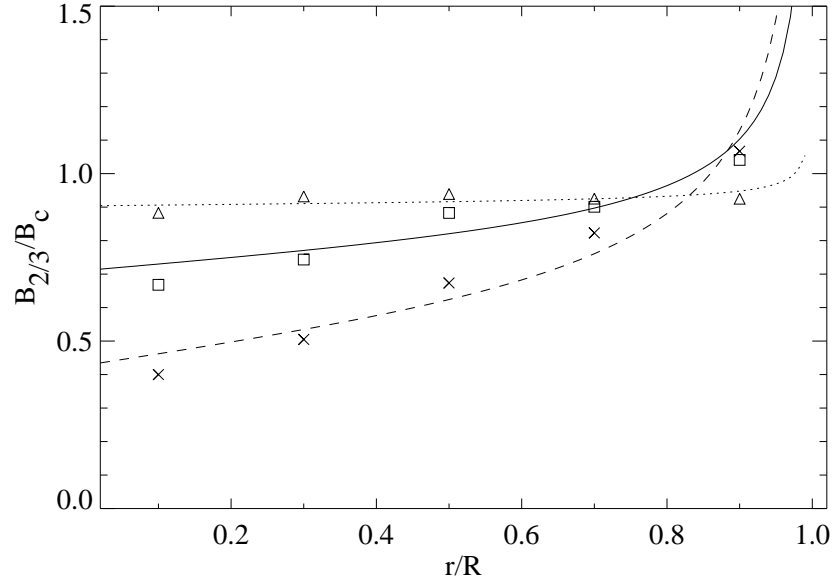


Figure 5. The ratio $B_{2/3}/B_c$ of the magnetic field at the distance of $2/3$ of the sunspot radius to the magnetic field at sunspot center as a function of heliocentric distance r/R for small sunspots (triangles and dotted line), transition sunspots (squares and solid line), and regular sunspots (crosses and dashed line). Symbols indicate median values computed for five intervals in r/R (in 0.2 step).

